Coverage Enhancements using RIS-Integrated NR

Visa Tapio*, Arman Shojaeifard†, Deepa Jagyasi†, Pekka Pirinen*, and Markku Juntti*
*Centre for Wireless Communications (CWC)
University of Oulu, Oulu, Finland
Email: FirstName.LastName@oulu.fi
†InterDigital Europe Ltd., London, UK
Email: FirstName.LastName@interdigital.com

***Abstract*—A reconfigurable intelligent surface (RIS) can be used to control the propagation of electromagnetic waves (EM). By deploying the RIS units in radio environment allows to steer the transmitted EM waves to areas that are otherwise shadowed by buildings or other geographic formations resulting in coverage enhancement. The gain offered by the RIS is due to its ability to focus the impinging signal to the desired direction. Hence, errors in the beamforming degrade the performance of a RIS-assisted link. The effect of the errors in the beamforming at the RIS are studied in this paper. Simulations show that the errors especially in the zenith angle can have significant effect on the uplink performance. With a RIS based on a 16×16 element reflect array errors greater than 1° start to limit the achievable throughput. After the RIS is configured based on the direction information, the user equipment must use a proper precoder to capitalize the benefit of the path via the RIS. The usability of existing precoders from the 5G NR are also studied in this paper. In the simulated use case, utilizing a RIS with 5G NR precoders resulted in 3.6 dB gain in the uplink direction.**

I. Introduction

Reconfigurable intelligent surface (RIS) is a programmable structure that can be used for controlling the propagation of electromagnetic (EM) waves by changing the electric and magnetic properties of the surface [1]. By placing RIS units into the environment where wireless systems are operating, the properties of the radio channels can be partially controlled [2]. The control over the propagation environment opens possibilities for improving the performance of wireless systems [3], [4], [5]. One application of the RIS is the coverage enhancement of wireless links where a RIS is used to enhance the signal-to-noise ratio (SNR) at the receiver [6]. In this paper, the RIS is used to enhance the uplink performance below 10 GHz frequency. Typically, the RIS is considered to be used at millimeter frequencies but its feasibility at sub-6 GHz frequencies has been demonstrated in [7], [8], [9].

In this work, a RIS is assumed to be a passive device in the sense that it does not amplify the signal but merely collects the arriving wave and reflects the impinging signal to the direction of the receiver. The RIS is used to enhance the coverage of a wireless communication system in a case where the direct link between a base station (BS) and a user equipment (UE) is severely shadowed or completely blocked. The RIS is deployed at a location where line-of-sight (LOS) channels exist between the RIS and both the UE and the BS. To maximize the SNR at the receiver, the radiation pattern of the RIS must be accurately directed.

In multiple-input, multiple-output (MIMO) wireless systems utilizing antenna arrays both at the BS and UE, the full utilization of the channel characteristics requires precoding at the transmitting node. This applies also for the RIS-assisted systems. The RIS configuration and precoder design has been considered, e.g., in [10], [11], [12] where precoders are calculated with the singular value decomposition (SVD) after the RIS configuration has been found based on channel estimation. A practical solution is to use predetermined codebooks for the precoding.

In this paper, the effect of the errors in the RIS configuration, resulting in misdirection of the RIS radiation pattern, on the link throughput is studied. Further, utilization of the existing 5G NR codebooks in the RIS assisted uplink is tested with simulations.

II. System Model

The considered system consisting of a 5G NR base station or g Node b (gNb), a UE and a $N \times M$-element RIS, where N and M are numbers of RIS elements in horizontal and vertical direction respectively, is illustrated in Fig. 1. The distances between the UE and the gNB, the UE and the RIS, the RIS and the gNB are marked with d_1, d_2 and d_3 and the corresponding power losses are denoted by A_1, A_2 and A_3, respectively. When a direct link exists between the UE and the gNB, the role of the RIS is to enhance the link performance. If the direct link is blocked completely, the RIS is needed to enable transmissions between the UE and the gNB.

The composite channel between the UE and the gNB can be written as

$$\mathbf{H} = \mathbf{H}_1 + \mathbf{H}_3 \mathbf{\Omega} \mathbf{H}_2. \tag{1}$$

where $\mathbf{H}_1$, $\mathbf{H}_2$, $\mathbf{H}_3$ and $\mathbf{\Omega}$ are the channels between the UE and the gNB, between the UE and the RIS, between the RIS and the gNB, and the RIS configuration matrix, respectively. Using geometric channel models as is in [13], [10] the model for the channel between the UE and the RIS becomes

$$\mathbf{H}_2 = \sum_{p=1}^{L_2} \alpha_{2,p} \mathbf{a}\left(\theta_{2,\text{RIS}}^{(p)}, \phi_{2,\text{RIS}}^{(p)}\right) \mathbf{a}^{\text{H}}\left(\theta_{2,\text{UE}}^{(p)}\right) \tag{2}$$

where L_2 is the number of paths between the UE and the RIS, $\alpha_{2,p}$ is the complex gain of the p^{th} path and $\theta_{2,\text{RIS}}^{(p)}$, $\phi_{2,\text{RIS}}^{(p)}$ and $\theta_{2,\text{UE}}^{(p)}$ are the angle-of-arrival (AoA) and the zenith-of-arrival (ZoA) at the RIS, and the angle-of-departure (AoD) at the UE

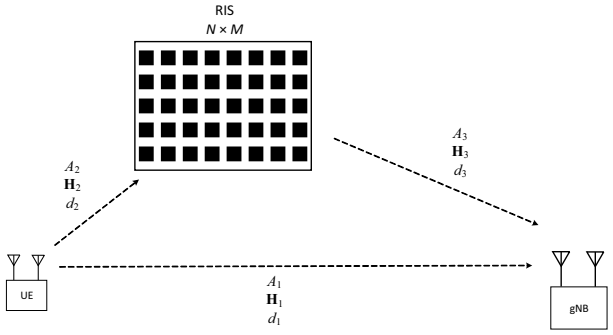

Fig. 1. RIS assisted wireless link.

of the p^{th} path, respectively. The array response vectors for the uniform linear arrays (ULA) at the UE and the gNB are defined as $\mathbf{a}(\theta) = \exp\left(i2\pi d/\lambda \boldsymbol{\vartheta} \sin\theta\right)$ ($\boldsymbol{\vartheta} = [0, 1, \cdots N_{\text{ant}} - 1]^{\text{T}}$), where N_{ant} is the number of antenna elements, λ is the wavelength, d is the antenna element spacing and θ is the AoA (DoA) at the gNB (UE). For the planar RIS, the response vector can be written as $\mathbf{a}(\theta, \phi) = \text{vec}(\psi(n, m))$ where

$$\psi(n, m) = \exp\left(\frac{2\pi}{\lambda}\left(n \sin\theta \cos\phi + m \sin\theta \cos\phi\right)\right) \quad (3)$$

and (n, m) is the position of an element in the planar RIS and $\text{vec}(\psi(n, m))$ is the vectorization of the matrix formed by the terms $\psi(n, m)$. The channel between the RIS and the gNB can be written as

$$\mathbf{H}_3 = \sum_{q=1}^{L_3} \alpha_{3,q} \mathbf{a}\left(\theta_{3,\text{gNB}}^{(q)}\right) \mathbf{a}^{\text{H}}\left(\theta_{3,\text{RIS}}^{(p)}, \phi_{3,\text{RIS}}^{(p)}\right) \quad (4)$$

where L_3 is the number of paths between the RIS and the gNB, $\alpha_{3,q}$ is the complex gain of the q^{th} path, and $\theta_{3,\text{gNB}}^{(q)}$, $\theta_{3,\text{RIS}}^{(q)}$ and $\phi_{3,\text{RIS}}^{(q)}$ are the AoA at the gNB, and zenith-of-departure (ZoD) and AoD at the RIS, respectively.

Similarly, the channel between the transmitter and the receiver can be written as

$$\mathbf{H}_1 = \sum_{t=1}^{L_1} \alpha_{1,t} \mathbf{a}\left(\theta_{1,\text{gNB}}^{(t)}\right) \mathbf{a}^{\text{H}}\left(\theta_{1,\text{UE}}^{(t)}\right) \quad (5)$$

where L_1 is the number of paths between the transmitter and receiver, $\alpha_{1,t}$ is the complex gain of the t^{th} path, and $\theta_{1,\text{gNB}}^{(t)}$, $\theta_{1,\text{UE}}^{(t)}$ are the AoA and AoD of the t^{th} path at the gNB and UE, respectively. The operation of the RIS is described with matrix $\boldsymbol{\Omega}$ whose diagonal elements are $\delta_{ii} = \alpha_{ii}\exp(i\omega_{ii})$ and α_{ii}, ω_{ii} are the absolute values and phases of the reflection coefficients of the RIS elements.

III. RIS Configuration and Precoding

In the case of uplink coverage enhancement, the RIS is used to increase the signal-to-noise ratio (SNR) at the receiving gNB. To maximize the SNR at the gNB, the RIS must form a beam and direct it to the gNB direction.

The signal-to-noise ratio (SNR) of the received signal at an antenna element of the receiving antenna array is

$$\gamma = \frac{|\sum_{n=1}^{N}\sum_{m=1}^{M} h_2^{(n,m)} h_3^{(n,m)} e^{-j\omega_{n,m}} x|^2}{\sigma^2}, \quad (6)$$

where σ^2 is the noise power and $h_2^{(n,m)}$ and $h_3^{(n,m)}$ are the components of the channels $\mathbf{H}_2$, $\mathbf{H}_3$ in the signal path via the RIS element (n, m).

When only one path exists between the transmitter and the RIS and between the RIS and the receiver, the SNR is maximized when the elements of the summation in the numerator of (6) add up coherently. Hence, the requirement for the SNR maximization is

$$\begin{aligned} &\arg(h_3^{(n,m)} h_2^{(n,m)}) - \omega_{n,m} = \Delta_\phi, \\ &\forall n \in [1, N],\ \forall m \in [1, M], \end{aligned} \quad (7)$$

where $\arg(\cdot)$ is the phase of the complex number inside the parentheses and $\Delta_\phi \in \mathbb{R}$ is any constant. The requirement for the phase of the RIS element (n, m) is then

$$\omega_{n,m} = \arg(h_3^{(n,m)} h_2^{(n,m)}) + \Delta_\phi,\ \forall n \in [1, N],\ \forall M \in [1, M]. \quad (8)$$

The same result for a uniform linear array (ULA) was derived as a solution to the lower bound maximization of the energy efficiency and rate in [14]. In the case of ULA based RIS, the channel vectors are $\mathbf{h}_2 = \mathbf{a}_{\text{in}} h_2$ and $\mathbf{h}_3 = \mathbf{a}_{\text{out}} h_3$ where $\mathbf{a}_{\text{in}}$ and $\mathbf{a}_{\text{out}}$ are the array response vectors for the impinging and reflected waves and h_2, h_3 are the complex channel gains. This leads to phase shift requirements for a ULA-based RIS as

$$\begin{aligned} \arg(h_3^{(n)} h_2^{(n)}) &= \arg(h_2 h_3 e^{j2\pi/\lambda n d(\sin\theta_{\text{out}} - \sin\theta_{\text{in}})} \\ &= \frac{2\pi}{\lambda} n d(\sin\theta_{\text{out}} - \sin\theta_{\text{in}}) + \arg(h_3 h_2) \end{aligned} \quad (9)$$

where θ_{in} and θ_{out} are the AoA and AoD at the ULA.

When there is only one path between the UE and the RIS and the RIS and the BS, the phase values to maximize the SNR can be found also by considering conventional antenna array steering. To maximize the power at the receiver, the RIS must form a narrow beam and direct it accurately towards the UE. When the RIS is implemented with a planar array, the RIS configuration depends on the AoA, ZoA, AoD and ZoD at the RIS. The definitions of ZoA and AoA angles are shown as θ and ϕ, respectively in Fig. 2. The ZoD and AoD are defined similarly. For the beamforming, the RIS elements must perform phase shifts for the signals impinging to the RIS element to steer the signal towards the BS. The required phase shift for an element at position (n, m) can be calculated as [15]

$$\begin{aligned} \Delta_\omega(n, m) =& \kappa d[n\left(\sin\theta_{3,\text{RIS}} \cos\phi_{3,\text{RIS}} - \sin\theta_{2,\text{RIS}} \cos\phi_{3,\text{RIS}}\right) \\ &+ m\left(\sin\theta_{3,\text{RIS}} \sin\phi_{3,\text{RIS}} - \sin\theta_{2,\text{RIS}} \sin\phi_{2,\text{RIS}}\right)] \end{aligned} \quad (10)$$

where $\kappa = 2\pi/\lambda$.

The gain offered by a passive RIS is based on its ability to focus the electromagnetic energy impinging on it to the

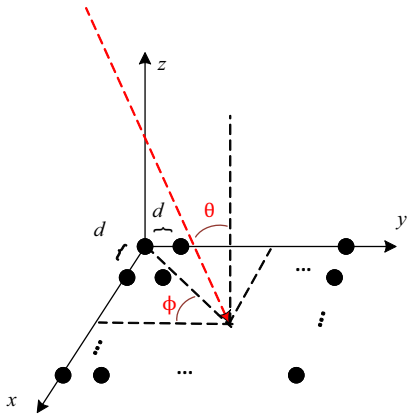

Fig. 2. Definition of angles.

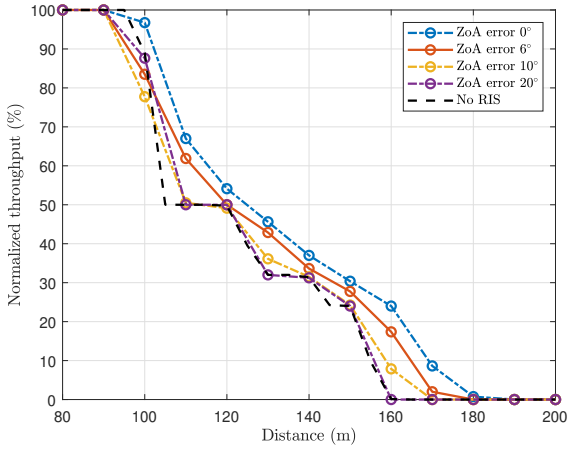

Fig. 3. Effect of the ZoA error (8×8 RIS, no error in AoA, AoD, ZoD).

correct direction. To be able to convey enough energy to the gNB to increase the SNR, the RIS must have a large number of elements, which in turn means that the beamwidth of the RIS is narrow. For example, the -3 dB beamwidth of a 16×16 reflect array with element spacing of $\lambda/2$ used in Section IV is about $6°$ and the beamwidth between the first nulls around the main beam is about $14°$ in both horizontal and vertical dimensions.

If the beam at the RIS is not accurately pointed to the correct direction, the gain offered by using the RIS decreases rapidly. The simulations showing the effect of the pointing error are reported in Section IV.

The RIS configuration alone does not guarantee the best possible link performance in MIMO systems but also the processing at the multi-antenna transmitter and receiver needs to be considered. After the RIS has been configured, the link quality at the receiver can be further improved by precoding at the UE. The 5G NR specification defines the precoders for the UE [16]. The precoder can be selected based on, e.g., signal-to-interference-and-noise ratio (SINR). Other metrics for the precoder selection include capacity, singular value, minimum mean square error, and mutual information [17].

IV. Numerical Examples

In the first example, the requirement for the accuracy of the direction information at the RIS is simulated with a 5G NR PUSCH simulator based on the model available in the 5G Toolbox in Matlab. The center frequency is 4 GHz, data modulation is quadrature phase shift keying (QPSK), the hybrid automatic repeat request (HARQ) is enabled, the sub-carrier spacing is 15 kHz and the number of resource blocks in the frequency domain is 52. Effect of errors in the direction setting with a 16×16 RIS on the normalized throughput in 5G NR physical uplink shared channel (PUSCH) transmission is shown in Fig. 7 and Fig. 8. In these cases, the fading channel $\mathbf{H}_1$ is modeled with the CDL-A model and the path loss is calculated with the urban micro – street canyon non-line-of-sight path loss model in [18]. The channels from the UE to the RIS and from the RIS to the gNB are one-tap LoS channels with indoor – office and urban micro – street path losses, respectively. The channel is estimated with the demodulation reference signal (DMRS) using the least squares (LS) channel estimator available in Matlab 5G Toolbox. Direction from the RIS to the gNB is assumed to be known.

RIS sizes 8×8, 10×10 and 16×16 are considered. In Figs. 3, 5 and 7, the AoA at the RIS is assumed to be known but there is an error in the ZoA angle resulting in an error in the RIS configuration, i.e., the RIS beam is steered off the correct direction due to the ZoA error. When the ZoA error in the 8×8 RIS case (Fig. 3) increases to $6°$ the throughput starts to decrease, but since the RIS provides only a slight gain over the case where no RIS is present in the system the effect of the error is also small. When the RIS size is increased to 10×10 (Fig. 5) and further to 16×16 (Fig. 7) it can be seen that the sensitivity to the ZoA error increases rapidly. However, since the increase of the RIS size also increases the gain, the largest RIS still provides more gain than the small ones even it is more sensitive to the ZoA error.

The error in AoA does not have as drastic effect as the ZoA error as can be seen in Figs. 4, 6 and 8. In the 16×16 case, the performance starts to deteriorate after the AoA error exceeds $5°$ while the ZoA error starts to affect the performance when it reaches $1°$. Hence, in the RIS-aided communication scenario, the achievable performance is highly sensitive to the errors introduced in ZoA at the RIS as compared to the errors in the AoA. This can be explained by noting that the error in the ZoA has a greater impact on the RIS element phase values in (10) than the error in AoA.

For utilizing 5G NR precoders, an example case has been simulated with a 16×16 RIS while assuming two antennas at the UE and gNB along with two number of layers at each. The distance between the UE and gNB is 180 m, between the UE and RIS is 5 m and between the RIS and gNB is 180 m. The AoA at the gNB antenna array is $30°$, AoA, ZoA, AoD and DoA at the RIS are $30°$, $30°$, $20°$ and $120°$, respectively. The ZoD and AoD are defined similarly. The element spacing (d in Fig. 2) of the RIS as well as in antenna arrays at the

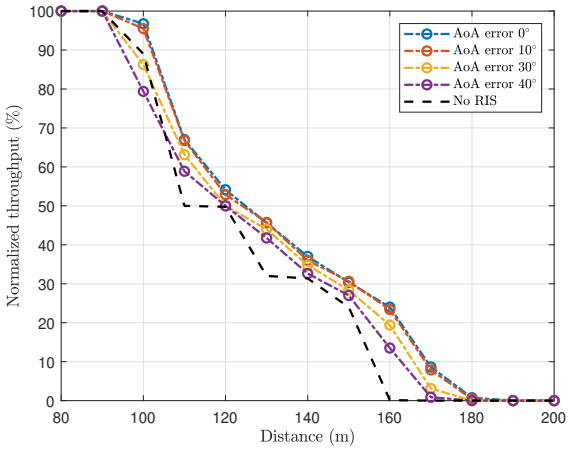

Fig. 4. Effect of the AoA error (8×8 RIS, no error in ZoA, AoD, ZoD).

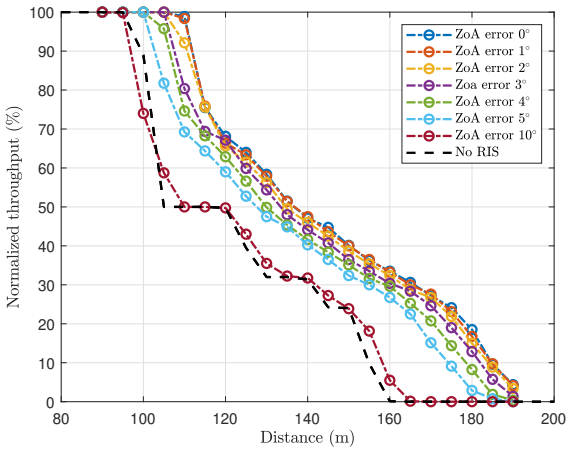

Fig. 5. Effect of the ZoA error (10×10 RIS, no error in AoA, AoD, ZoD).

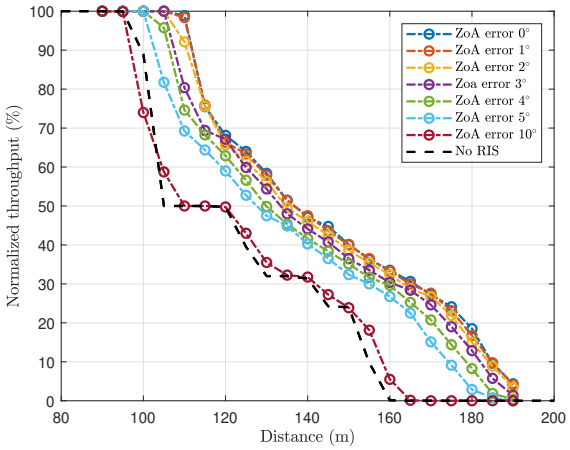

Fig. 6. Effect of the AoA error (10×10 RIS, no error in ZoA, AoD, ZoD).

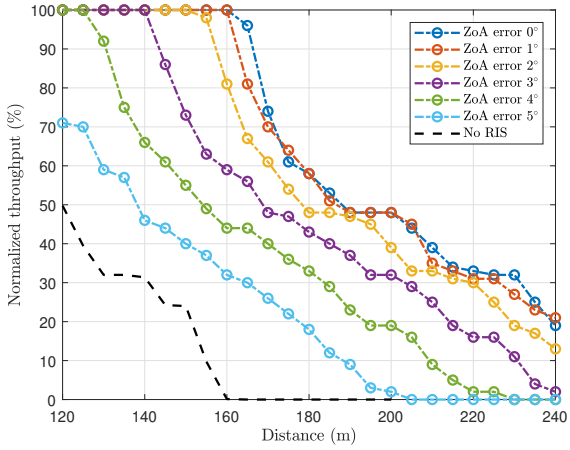

Fig. 7. Effect of the ZoA error (16×16 RIS, no error in AoA, AoD, ZoD).

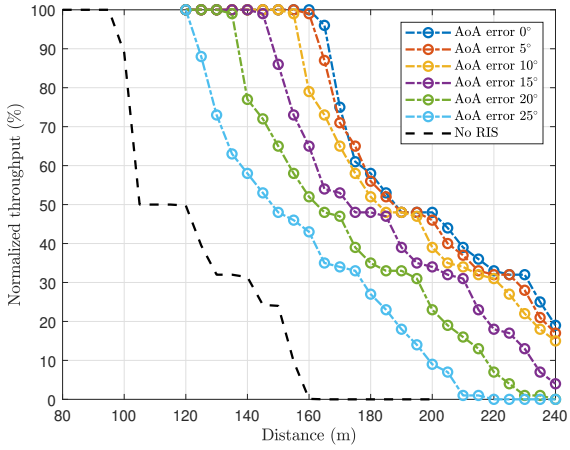

Fig. 8. Effect of the AoA error (16×16 RIS, no error in ZoA, AoD, ZoD).

UE and the gNB is considered as $\lambda/2$ ($\lambda =$ wavelength). The selected precoder matrix indicators (PMI) are shown in Fig. 9. The PMIs have been calculated separately for each resource block at every slot and the used codebook is for the two-layer transmission using two antenna ports with transform precoding disabled defined in [16]. The resulting SINR values using the PMIs of Fig. 9 at the gNB receiver are shown in Fig. 10. When averaged over the time (slot) and frequency (resource block) domain, the average SINR without and with the RIS is 6.5 dB and 10.1 dB, respectively. This means that the RIS in this case has offered 3.6 dB gain.

V. Conclusion

By placing a RIS at a proper location, it can be used to direct the signal transmitted by a UE around obstacles shadowing the link between a UE and a gNB, hence providing enhanced 5G NR uplink coverage. Since the RIS is a passive device, i.e., it does not include any amplifiers, the steering of the RIS beam pattern accurately to the correct direction is crucial in RIS assisted links if the full gain offered by the RIS is to be

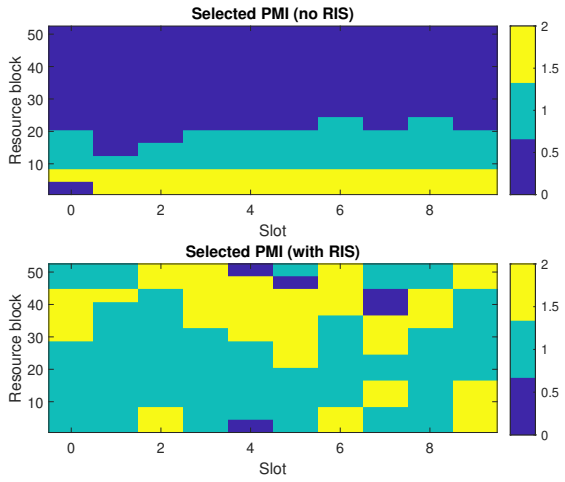

Fig. 9. Precoder indicators without and with the 16 × 16 RIS.

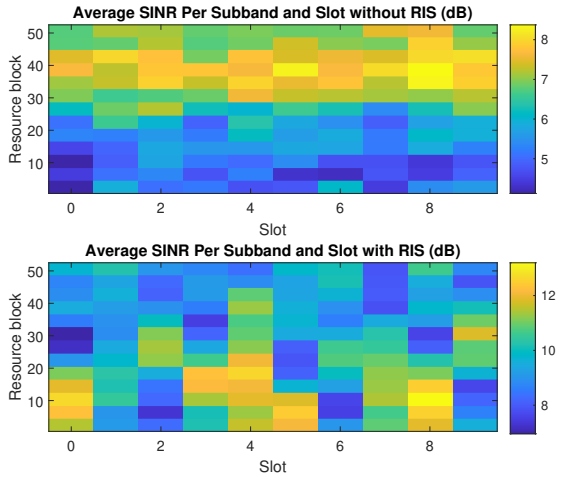

Fig. 10. Comparison of SINR without and with 16 × 16 RIS.

capitalized. However, even a large RIS is more sensitive to the pointing error than smaller ones the effects of the pointing errors are partially compensated by its large array gain.

The RIS configuration only does not automatically lead to the desired improvement in the link performance. The transmitting UE must also be able to select a proper precoder to steer its transmission so that the RIS can be utilized in the transmission. The 5G NR readily includes precoders and in the simulated case the uplink SNR was improved by 3.6 dB with the standard codebook even though the codebook has not been developed to be used with a RIS.

ACKNOWLEDGMENT

This research has been supported by the Academy of Finland, 6G Flagship program under Grant 346208. This work was developed in part within the CELTIC-NEXT European collaborative R&D project AIMM (ID: C2019/2-5).

REFERENCES

[1] M. Di Renzo, A. Zappone, M. Debbah, M.-S. Alouini, C. Yuen, J. de Rosny, and S. Tretyakov, "Smart radio environments empowered by reconfigurable intelligent surfaces: How it works, state of research, and the road ahead," *IEEE Journal on Selected Areas in Communications*, vol. 38, no. 11, pp. 2450–2525, 2020.

[2] Q. Wu and R. Zhang, "Towards smart and reconfigurable environment: Intelligent reflecting surface aided wireless network," *IEEE Communications Magazine*, vol. 58, no. 1, pp. 106–112, 2020.

[3] M. Toumi and A. Aijaz, "System performance insights into design of RIS-assisted smart radio environments for 6G," in *2021 IEEE Wireless Communications and Networking Conference (WCNC)*, 2021, pp. 1–6.

[4] E. C. Strinati, G. C. Alexandropoulos, H. Wymeersch, B. Denis, V. Sciancalepore, R. D'Errico, A. Clemente, D.-T. Phan-Huy, E. De Carvalho, and P. Popovski, "Reconfigurable, intelligent, and sustainable wireless environments for 6G smart connectivity," *IEEE Communications Magazine*, vol. 59, no. 10, pp. 99–105, 2021.

[5] E. Basar and H. V. Poor, "Present and future of reconfigurable intelligent surface-empowered communications [perspectives]," *IEEE Signal Processing Magazine*, vol. 38, no. 6, pp. 146–152, 2021.

[6] M. Nemati, J. Park, and J. Choi, "RIS-assisted coverage enhancement in millimeter-wave cellular networks," *IEEE Access*, vol. 8, pp. 188 171–188 185, 2020.

[7] X. Pei, H. Yin, L. Tan, L. Cao, Z. Li, K. Wang, K. Zhang, and E. Björnson, "RIS-aided wireless communications: Prototyping, adaptive beamforming, and indoor/outdoor field trials," *IEEE Transactions on Communications*, vol. 69, no. 12, pp. 8627–8640, 2021.

[8] B. G. Kashyap, P. C. Theofanopoulos, A. S. Shekhawat, A. Y. Modi, A. P. Sengar, S. K. Kumar, A. Chang, T. Osman, A. Alkhateeb, and G. C. Trichopoulos, "A reconfigurable intelligent surface for 5G wireless communication applications," in *2021 IEEE International Symposium on Antennas and Propagation and USNC-URSI Radio Science Meeting (APS/URSI)*, 2021, pp. 111–112.

[9] A. Araghi, M. Khalily, M. Safaei, A. Bagheri, V. Singh, F. Wang, and R. Tafazolli, "Reconfigurable intelligent surface (RIS) in the sub-6 GHz band: Design, implementation, and real-world demonstration," *IEEE Access*, vol. 10, pp. 2646–2655, 2022.

[10] J. He, H. Wymeersch, and M. Juntti, "Channel estimation for RIS-aided mmWave MIMO systems via atomic norm minimization," *IEEE Transactions on Wireless Communications*, vol. 20, no. 9, pp. 5786–5797, 2021.

[11] A. Zappone, M. Di Renzo, F. Shams, X. Qian, and M. Debbah, "Overhead-aware design of reconfigurable intelligent surfaces in smart radio environments," *IEEE Transactions on Wireless Communications*, vol. 20, no. 1, pp. 126–141, 2021.

[12] Z. Zhou, N. Ge, Z. Wang, and L. Hanzo, "Joint transmit precoding and reconfigurable intelligent surface phase adjustment: A decomposition-aided channel estimation approach," *IEEE Transactions on Communications*, vol. 69, no. 2, pp. 1228–1243, 2021.

[13] J. He, M. Leinonen, H. Wymeersch, and M. Juntti, "Channel estimation for RIS-aided mmWave MIMO systems," in *GLOBECOM 2020 - 2020 IEEE Global Communications Conference*, 2020, pp. 1–6.

[14] A. Zappone, M. Di Renzo, F. Shams, X. Qian, and M. Debbah, "Overhead-aware design of reconfigurable intelligent surfaces in smart radio environments," *IEEE Transactions on Wireless Communications*, vol. 20, no. 1, pp. 126–141, 2021.

[15] V. Tapio, A. Shojaeifard, I. Hemadeh, A. Mourad, and M. Juntti, "Reconfigurable intelligent surface for 5G NR uplink coverage enhancement," in *2021 IEEE 94th Vehicular Technology Conference (VTC2021-Fall)*, 2021, pp. 1–5.

[16] 3GPP, "3rd generation partnership project; technical specification group radio access network; nr; physical channels and modulation," 3GPP, 3GPP TS 38.211, V16.3.0, Release 16, 2020.

[17] T. Akyıldız and T. M. Duman, "Search-free precoder selection for 5G new radio using neural networks," in *2020 IEEE International Black Sea Conference on Communications and Networking (BlackSeaCom)*, 2020, pp. 1–6.

[18] 3GPP, "Study on channel model for frequencies from 0.5 to 100 GHz," ETSI, 3GPP TR 38.901, version 14.3.0, Release 14, 2018. [Online]. Available: https://www.etsi.org/deliver/etsi_tr/138900_138999/138901/14.03.00_60/tr_138901v140300p.pdf